ACS APPLIED MATERIALS & INTERFACES

Research Article

www.acsami.org

Biocompatible Nanocarrier Fortified with a Dipyridinium-Based Amphiphile for Eradication of Biofilm

Sudeep Goswami,[†] Durairaj Thiyagarajan,[†] Gopal Das,*[,‡] and Aiyagari Ramesh*[,†]

[†]Department of Biotechnology, Indian Institute of Technology Guwahati, Guwahati 781039, India

[‡]Department of Chemistry, Indian Institute of Technology Guwahati, Guwahati 781039, India

Supporting Information

ABSTRACT: Annihilation of bacterial biofilms is challenging owing to their formidable resistance to therapeutic antibiotics and thus there is a constant demand for development of potent antibiofilm agents that can abolish established biofilms. In the present study, the activity of a dipyridinium-based cationic amphiphile (**compound 1**) against established bacterial biofilms and the subsequent development of a **compound 1**-loaded nanocarrier for potential antibiofilm therapy are highlighted. Solution-based assays and microscopic analysis revealed the antagonistic effect of **compound 1** on biofilms formed by *Staphylococcus aureus* MTCC 96 and *Pseudomonas aeruginosa* MTCC 2488. In combination studies, **compound 1** could efficiently potentiate the action of tobramycin and gentamicin on *P. aeruginosa* and *S. aureus* biofilm, respectively. A human serum albumin (HSA)-based nanocarrier loaded with **compound 1** was generated, which exhibited sustained release of **compound 1** at physiological pH. The **compound 1**-loaded HSA nanocarrier (C1-HNC) displayed the signature membrane-directed activity of the amphiphile on target bacteria, efficiently eliminated established bacterial biofilms, and was observed to be nontoxic to a model human cell line. Interestingly, **compound 1** as well as the amphiphile-loaded HSA nanocarrier could eradicate established *S. aureus* biofilm from the surface of a Foley's urinary catheter. On the basis of its biocompatibility and high antibiofilm activity, it is conceived that the amphiphile-loaded nanocarrier may hold potential in antibiofilm therapy.

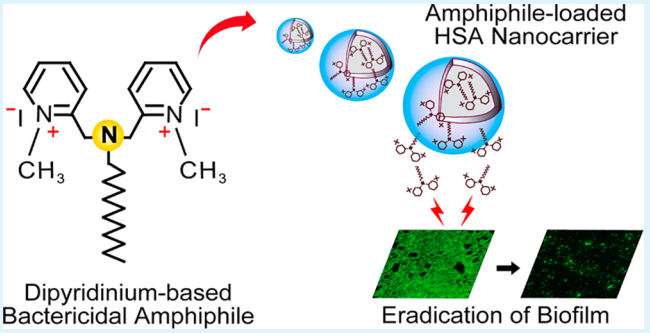

KEYWORDS: *amphiphile, HSA nanocarrier, antibacterial, antibiofilm, antibiotic, catheter*

INTRODUCTION

Bacterial biofilms constitute a highly organized cluster of cells that display an inherent ability of adhesion to a surface and elaborate an extracellular polymeric matrix that shields the embedded cells.[1−5] Biofilm formation is considered as an alternate lifestyle adopted by microorganisms that facilitates importunate survival of the cells in diverse and harsh niche.[1,6] Among various bacterial strains, the most commonly encountered and clinically relevant biofilm-forming bacteria include *Staphylococcus aureus*, *Staphylococcus epidermidis*, and *Pseudomonas aeruginosa*.[7,8] Biofilms are associated with an overwhelming number of microbial infections, with periodontitis, endocarditis, and chronic lung infections in cystic fibrosis patients being the prominent ailments.[5,9−12] Furthermore, given their propensity to colonize indwelling medical devices such as vascular and urinary catheters, bacterial biofilms are significant players in device-associated infections.[13−15]

Treatment of biofilm-associated chronic infections is confronted with the vexing challenge of eliminating matrix-embedded sessile bacteria, which are known to be remarkably resistant to the action of conventional therapeutic antibiotics.[4,16] The extracellular polymeric matrix of biofilms is acknowledged as a barrier for diffusion of antibiotics.[3,4,6,7] Further, the presence of metabolically inactive persister cells in biofilm leads to development of resistance against antibiotics, which are known to act on growing cells.[17,18] Owing to the grave healthcare concern associated with bacterial biofilms, development of various synthetic agents that effectively inhibit biofilm formation have been proposed.[19−23] However, from a clinical standpoint, a significant challenge is the mitigation of chronic infections caused by established biofilms, which are highly refractory to the action of common therapeutic antibiotics.[4] The crux of the problem is in the availability of molecules that can display antagonistic activity in the complex niche of the biofilm matrix and annihilate mature biofilms. In this context, synthetic bactericidal scaffolds that can penetrate the biofilm matrix and act on profound bacterial targets such as the membrane are potential candidates. To this end, low molecular weight synthetic cationic amphiphiles can be considered as a viable option as it is conceived that such amphiphiles are likely to infiltrate through the biofilm matrix, access the encased cells owing to their proclivity to interact with anionic bacterial cell surface and render extensive membrane damage.[24−26] Furthermore, owing to their mem-

Received: July 20, 2014
Accepted: August 27, 2014
Published: August 27, 2014

brane-targeting activity, amphiphiles can perhaps act as an adjuvant to potentiate the action of antibiotics in combination therapy.[25]

A critical parameter, which is likely to impact the potential of synthetic bactericidal amphiphiles in antibiofilm therapy, is the development of an effective delivery system that can ensure sustained release of the amphiphile. In this direction, development of nanocarriers for entrapment and controlled release of potentially therapeutic antibacterial amphiphiles can be conceived as a rational approach. The utility of nanomaterials for efficient delivery of antibacterials and development of antibiofilm agents is well documented.[27−32] Protein-based nanocarriers are perceived as suitable delivery vehicles owing to their superior permeation and retention effect, biocompatibility, and biodegradability.[33,34] In this regard, serum albumin is suitable for the development of nanocarriers based on its nonimmunogenic, biodegradable, and nontoxic nature and high encapsulation efficiency.[35,36]

On the basis of the aforementioned rationale, herein we report the activity of a membrane-acting dipyridinium-based synthetic amphiphile referred to as **compound 1** on established bacterial biofilms. Studies revealed that the amphiphile alone as well as in combination with antibiotics could effectively abolish established biofilms of *S. aureus* and *P. aeruginosa*. A human serum albumin (HSA)-based nanocarrier loaded with **compound 1** was generated, which displayed potent antibacterial and antibiofilm activity and was nontoxic to a model human cell line. Interestingly, the amphiphile alone as well as amphiphile-loaded HSA nanocarrier could be applied in model experiments to demonstrate significant eradication of established *S. aureus* biofilm from the surface of a urinary catheter.

EXPERIMENTAL PROCEDURES

Materials. Nutrient Broth (NB), Brain-Heart Infusion (BHI) broth, and crystal violet (CV) dye were procured from HiMedia (India). Dimethyl sulfoxide (DMSO), absolute ethanol, and glutaraldehyde were obtained from Merck (India). *N*-2-Hydroxyethyl piperazine *N*-2 ethanesulfonic acid (HEPES buffer) was procured from Sisco Research Laboratories (India). Five (and 6)-carboxyfluorescein diacetate succinimidyl ester (cFDA-SE), propidium iodide (PI), congo red (CR), gentamicin, tobramycin, human serum albumin (HSA, Fraction V, purity 96−99%), 3,3′-dipropylthiadicarbocyanine iodide ($DiSC_3 5$), valinomycin, Dulbecco's Modified Eagle Medium (DMEM), trypsin-EDTA, 3-(4,5-dimethyl-2-thiazolyl)-2,5-diphenyl-2H-tetrazolium bromide (MTT), paraformaldehyde, and Triton X-100 were procured from Sigma-Aldrich. A Foley's urinary catheter was procured from Sisco Latex Pvt. Ltd. (India).

Compound 1. In the present study, the synthetic cationic amphiphile *N*,*N*-bismethyl ((pyridinium-2-yl) methyl iodide) alkylamine referred to as **compound 1** was used. In an earlier study conducted with several pyridine-based amphiphiles, this amphiphile was referred to as **compound 6**, and its synthesis and characterization was reported.[25] The general structure of **compound 1** is indicated in Figure 1A. A 10 mg/mL (~15.35 mM) stock solution of **compound 1** was prepared in DMSO and stored at room temperature under dark conditions.

Bacterial Strains and Growth Conditions. In the present study, Gram-positive bacteria *Staphylococcus aureus* MTCC 96 (*S. aureus*) and *Listeria monocytogenes* Scott A (*L. monocytogenes*) and Gram-negative bacteria *Escherichia coli* MTCC 433 (*E. coli*), *Enterobacter aerogenes* MTCC 2822 (*E. aerogenes*), and *Pseudomonas aeruginosa* MTCC 2488 (*P. aeruginosa*) were used. *S. aureus* MTCC 96 and *L. monocytogenes* Scott A were cultured in Brain-heart Infusion (BHI) broth at 37 °C and 180 rpm for 12 h. *E. coli* MTCC 433, *E. aerogenes* MTCC 2822, and *P. aeruginosa* MTCC 2488 were propagated in Nutrient Broth (NB) at 37 °C and 180 rpm for 12 h. All the bacterial strains were grown from frozen stocks and subcultured prior to their use in experiments.

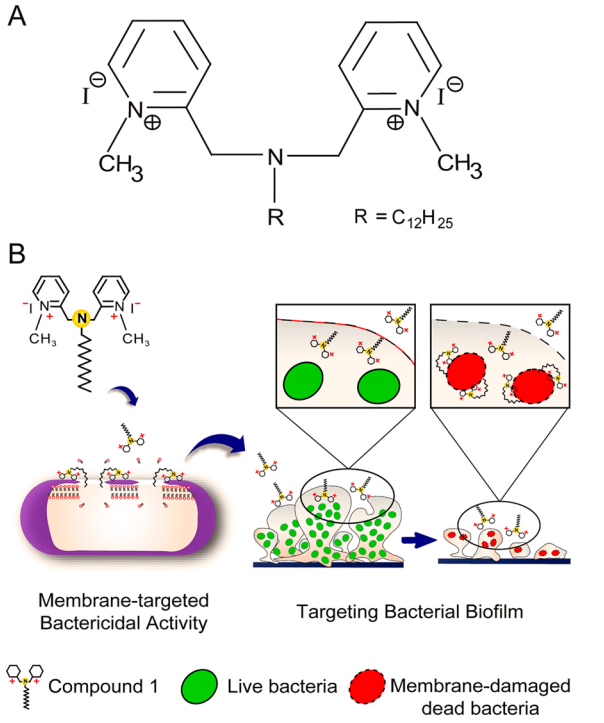

Figure 1. (A) General structure of **compound 1**. (B) Cartoon illustrating the potential antibiofilm activity of the membrane-acting **compound 1**.

Minimum Inhibitory Concentration (MIC) of Compound 1, Gentamicin, and Tobramycin. The MIC of **compound 1**, gentamicin, and tobramycin against the target bacteria was determined by a standard method described in the Supporting Information.

Antibiofilm Activity of Compound 1. Biofilms of *S. aureus* MTCC 96 and *P. aeruginosa* MTCC 2488 were grown in sterile 96 well microtiter plates following a standard method (see the Supporting Information). The antibiofilm activity of **compound 1** against established *S. aureus* MTCC 96 biofilm and *P. aeruginosa* MTCC 2488 biofilm was ascertained by estimation of (a) viability by MTT assay, (b) biomass by crystal violet staining, and (c) extra-polymeric substance (EPS) by congo red staining. The antibiofilm activity of **compound 1** was also determined by atomic force microscope (AFM), fluorescence microscopy, and field emission scanning electron microscopy (FESEM) analysis. A detailed description of the aforementioned experiments is provided in the Supporting Information.

Anti-Biofilm Activity of Gentamicin and Tobramycin in Combination with Compound 1. Biofilms of *S. aureus* MTCC 96 and *P. aeruginosa* MTCC 2488 were grown in sterile 96 well microtiter plate following a standard method (see the Supporting Information). The established *S. aureus* biofilm was subsequently incubated with varying combinations of gentamicin (5.0−30 μg/mL) and **compound 1** (3 μM, 6 μM, 9 μM, 12 μM, and 15 μM), while *P. aeruginosa* biofilm was treated with tobramycin (0.08−0.625 μg/mL) and **compound 1** (10 μM, 20 μM, and 30 μM) for 24 h at 37 °C in a humid chamber. Subsequently the treated as well as control biofilm samples (untreated) were analyzed by crystal violet staining, congo red staining, and FESEM analysis (see the Supporting Information). The potential cytotoxic effect of the combination of tobramycin and **compound 1** was also ascertained by a standard MTT assay on cultured HeLa cells (see the Supporting Information).

HSA Nanoparticle (HNP) and Compound 1-Loaded HSA Nanocarrier (C1-HNC). Preparation of HNPs was accomplished by a desolvation method (see the Supporting Information). For generation of **compound 1**-loaded HSA nanocarrier (C1-HNC), HNPs (1.0 mg/

mL in sterile Milli-Q water, pH titrated to 8.2) were interacted overnight with varying concentrations of **compound 1** (5.0−800 μM) on a rocker at room temperature. Following incubation, the solution was centrifuged at 10 000*g* for 5 min. The pellet representing C1-HNC was resuspended in sterile Milli-Q water (pH titrated to 8.2). HNP and C1-HNC was characterized by FESEM, transmission electron microscopy (TEM), UV−visible spectroscopy, and FTIR analysis (see the Supporting Information). The loading capacity (LC) of HNPs and encapsulation of **compound 1** in HNPs was also determined (see the Supporting Information).

***In Vitro* Release Kinetics of Compound 1 from C1-HNC.** To study the *in vitro* release kinetics of **compound 1**, C1-HNC loaded with 125 μM of **compound 1** was dispersed in separate sets in 1.0 mL of 10 mM HEPES buffer (pH 7.4) and 100 mM citrate buffer (pH 3.0), respectively. The samples were incubated in an orbital shaker at 120 rpm at 37 °C. At specific time intervals (1 h, 3 h, 6 h, 12 h, 24 h, 48 h, and 72 h) the samples were withdrawn and centrifuged at 10 000*g* for 5 min. The supernatant from various samples were transferred into a fresh microcentrifuge tube, and UV−visible absorbance of the solutions was measured at 265 nm in a spectrophotometer. The absorbance value at 265 nm and a previously generated calibration curve for **compound 1** (see the Supporting Information) was used to measure the quantity of **compound 1** released from C1-HNC at specific time periods and expressed as % cumulative release.

Antibacterial Activity of C1-HNC. A series of experiments were conducted to determine the antibacterial activity of C1-HNC. These experiments included (a) time-kill curve, (b) TEM analysis, and (c) membrane depolarization assay. A detailed description of these experiments is provided in the Supporting Information.

Antibiofilm Activity of C1-HNC. Biofilm of *S. aureus* MTCC 96 was grown in a sterile 96 well microtiter plate following a standard method (see the Supporting Information) and treated in separate sets with various samples of HNP-C1 composite (corresponding to 5.0 μM, 10 μM, 15 μM, 20 μM, 25 μM, 30 μM, and 45 μM of **compound 1**) for 24 h. In a parallel control experiment, *S. aureus* MTCC 96 biofilm was also treated with HNPs alone. Following incubation, the wells were washed with sterile phosphate-buffered saline (PBS) and an MTT-based viability assay was performed for both C1-HNC-treated and HNP-treated samples (see the Supporting Information).

Eradication of Biofilm from Catheter Surface. The potential of **compound 1** and C1-HNC to eradicate catheter-associated biofilm was determined by a quantitative MTT assay. Biofilm of *S. aureus* MTCC 96 was grown over Foley's urinary catheter by incubating 1.0 cm × 0.5 cm segmented pieces of the catheter in a sterile tissue culture petridish (35 mm diameter) containing BHI broth with 0.25% glucose and the bacterial cell suspension (~10^7 CFU/mL) for 24 h in static and humid conditions under 37 °C. Following incubation, catheter segments colonized with *S. aureus* biofilm were recovered aseptically and rinsed gently with sterile PBS to remove unbound bacterial cells. The catheters were then transferred to separate sterile tissue culture petridish containing fresh media incorporated with varying concentrations of either **compound 1** or C1-HNC (corresponding to 5.0 μM, 10 μM, 15 μM, 20 μM, 25 μM, 30 μM, and 45 μM **compound 1**) and incubated for 24 h. Subsequently, the catheter segments were harvested, gently rinsed in sterile PBS, and further incubated in fresh sterile BHI media containing MTT reagent (0.5 mg/mL). After incubation for 4 h at 37 °C, the samples were washed thrice with sterile PBS to remove all traces of MTT. The purple colored formazan crystals were dissolved in DMSO for 15 min with brief mixing, and the absorbance of a 100 μL aliquot was measured at 550 nm using a microtiter plate reader (Infinite M200, TECAN, Switzerland). Each assay was performed in triplicate, and the results were expressed as the mean of three independent experiments. In order to prepare catheter specimens with bacterial biofilm for FESEM analysis, segments of the catheter were incubated into separate tubes containing 1.0 mL of BHI broth with 0.25% glucose and the bacterial cell inoculum (~10^7 CFU/mL *S. aureus*) for 24 h in static and humid condition under 37 °C. Subsequently, the catheter segments with pregrown *S. aureus* biofilm were incubated in separate sets in fresh requisite media incorporated with 30 μM **compound 1** or C1-HNC (representing 30 μM **compound 1**) for 24 h. Following treatment, the catheter segments were gently removed, rinsed with sterile Milli-Q water, and fixed with 2.5% glutaraldehyde for 1 h at room temperature followed by further rinsing with sterile Milli-Q water and drying. Samples representing the bare catheter segment (devoid of any biofilm growth) and the untreated catheter segment with established *S. aureus* biofilm were also fixed similarly. Subsequently, all the processed catheter segments were examined in a field emission scanning electron microscope (Zeiss Sigma) and their images were recorded.

Cytotoxic Effect of C1-HNC. Cytotoxicity of C1-HNC was assessed *in vitro* against the HeLa cell line by a standard MTT-based colorimetric assay following the manufacturer's instructions (Sigma-Aldrich). The cells were initially grown in a 25 cm^2 tissue culture flask in Dulbecco's Modified Eagle Medium (DMEM) supplemented with 10% (v/v) fetal bovine serum (FBS), penicillin (100 μg/mL), and streptomycin (100 μg/mL) at 37 °C under a humidified atmosphere of 5% CO_2 in an incubator. The cells were subsequently seeded onto 96-well tissue culture plates at a density of 10^4 cells per well and incubated with C1-HNC (corresponding to 5.0 μM, 10 μM, 15 μM, 20 μM, 25 μM, 30 μM, and 45 μM **compound 1**) for a period of 24 h. Untreated cells and cells treated with HSA nanoparticles were also incubated in parallel sets. Following incubation, the media was carefully aspirated and fresh DMEM medium containing MTT solution was added to the wells and the plates were incubated for 4 h at 37 °C. Subsequently, the supernatant was aspirated and the insoluble formazan product was solubilized in DMSO and its absorbance was measured in a microtiter plate reader (Infinite M200, TECAN, Switzerland) at 550 nm. The MTT assay was performed in six sets for each sample. The absorbance obtained for untreated cells was assumed to represent 100% cell viability, and the absorbance for other samples was compared to that obtained for untreated cells in order to determine % cell viability. Data analysis and determination of standard deviation were performed with Microsoft Excel 2010 (Microsoft Corporation).

For fluorescence microscope analysis, HeLa cells were seeded onto 96 well tissue culture plates (approximately 10^4 cells per well) and propagated in a CO_2 incubator as mentioned before to achieve 80% confluency. Subsequently, the cells were incubated with 30 μM of C1-HNC made in DMEM for a period of 24 h. Control samples (HeLa cells treated with HNPs alone) were also incubated in separate wells. In parallel sets, HeLa cells were fixed with 4% paraformaldehyde for 10 min at room temperature followed by treatment with 0.1% Triton X-100 for 10 min to achieve permeabilization of the cells. Cells belonging to all the experimental samples (HNP-treated cells, C1-HNC-treated cells, and Triton X-100 treated cells) were thoroughly washed with sterile PBS and labeled in separate sets with either 50 μM cFDA-SE or 30 μM PI each for 15 min, respectively. The cells were subsequently washed with sterile PBS, and images of the cells were captured using a fluorescence microscope (Eclipse Ti-U, Nikon) with a filter that allowed blue light excitation at 445−495 nm for cFDA-SE and green light excitation at 495−570 nm in the case of PI stained cells.

RESULTS AND DISCUSSION

Antibiofilm Activity of Compound 1. In the context of antibiofilm therapy, elimination of matrix-entrenched sessile bacteria, which defy the action of common therapeutic antibiotics,[4] is a significant challenge. The extracellular matrix in biofilms largely consisting of viscous polymeric substances constitutes a prominent diffusion barrier and has been implicated in sequestration and reduced bioavailability of antibiotics.[3] Given the high incidence of biofilm-associated chronic infections, antibiofilm agents that are capable of surmounting this matrix-associated impediment and disrupt established biofilms are thus in great demand. Synthetic bactericidal molecules that can infiltrate the biofilm matrix to establish contact with the entrenched cells and target the membrane bilayer emerge as potential candidates to accomplish this function. In an earlier study we demonstrated that the

cationic **compound 1** (Figure 1A) was a potent antibacterial and unlike many antibiotics, which act on intracellular targets, **compound 1** can interact with bacterial cells and trigger extensive membrane disruption.[25] It was thus envisaged that this cationic amphiphile could perhaps be explored for eradication of preformed biofilms as it is likely to permeate through the biofilm matrix, interact with the underlying anionic bacterial cells, and render large-scale membrane damage in cells (Figure 1B). To verify this rationale, bacterial biofilm was grown in microtiter wells and then treated with varying concentrations of **compound 1**. A standard crystal violet-based colorimetric assay for biofilm biomass suggested a significant eradication of *S. aureus* and *P. aeruginosa* biofilm, which could be correlated with the dose of **compound 1** (Figure 2A,B). It is to be noted that the concentration of the amphiphile required for elimination of *P. aeruginosa* biofilm was many fold higher compared to *S. aureus* biofilm. This can perhaps be attributed to the intrinsic resistance typically associated with *P. aeruginosa*.[37] The concentration-dependent eradication of preformed biofilms of *S. aureus* and *P. aeruginosa* by **compound 1** was corroborated by an MTT assay (Supporting Information, Figure S1A,B). Obliteration of the established biofilm by **compound 1** was also validated by a congo red binding assay, which illustrated a dose-dependent reduction of biofilm EPS matrix upon treatment with **compound 1** (Supporting Information, Figure S1C,D).

AFM imaging of *S. aureus* and *P. aeruginosa* biofilms was pursued to further evaluate the antibiofilm potential of **compound 1**. In the case of untreated samples (control), compact protrusions and surface corrugations typically associated with dense biofilm architecture were evident in the three-dimensional topographic images (Figure 2C,D), amplitude channel, and two-dimensional topographic images (Supporting Information, Figure S2A,B). The average height profiles for untreated *S. aureus* and *P. aeruginosa* biofilms were approximately ∼508 nm and ∼632 nm, respectively (Supporting Information, Figure S2A,B). AFM images of *S. aureus* and *P. aeruginosa* biofilms treated with 30 μM and 200 μM **compound 1**, respectively, indicated prominent abrasion of the biofilm structure and disaggregation of the cells (Figure 2C,D and the Supporting Information, Figure S2A,B), corroborated by a dramatic reduction in the average height profile, which was observed to be ∼72 nm and ∼237 nm for *S. aureus* and *P. aeruginosa* biofilm, respectively (Supporting Information, Figure S2A,B). Fluorescence microscopy analysis revealed a dense network of cFDA-SE stained *S. aureus* and *P. aeruginosa* biofilm, indicating the presence of viable and metabolically active cells in untreated biofilm (Figure 2E,F). However, upon treatment with the amphiphile, the biofilm architecture was significantly disintegrated (Figure 2E,F). In FESEM analysis, it was evident that the organized cluster of cells exhibiting distinct cell−cell adhesion in the case of untreated *S. aureus* biofilm was severely impaired upon treatment with 30 μM **compound 1**, wherein the cells lost their typical morphology and integrity (Supporting Information, Figure S3). Eradication of *S. aureus* biofilm by **compound 1** was also observed through a dramatic reduction in the formation of extracellular EPS as ascertained by congo red staining (Supporting Information, Figure S3). Furthermore, it was observed that **compound 1**-treated *S. aureus* biofilm displayed notable PI staining (Supporting Information, Figure S3), which suggested that the amphiphile could permeate through the extracellular biofilm matrix to reach the embedded cells and render large-scale membrane damage. Analogous

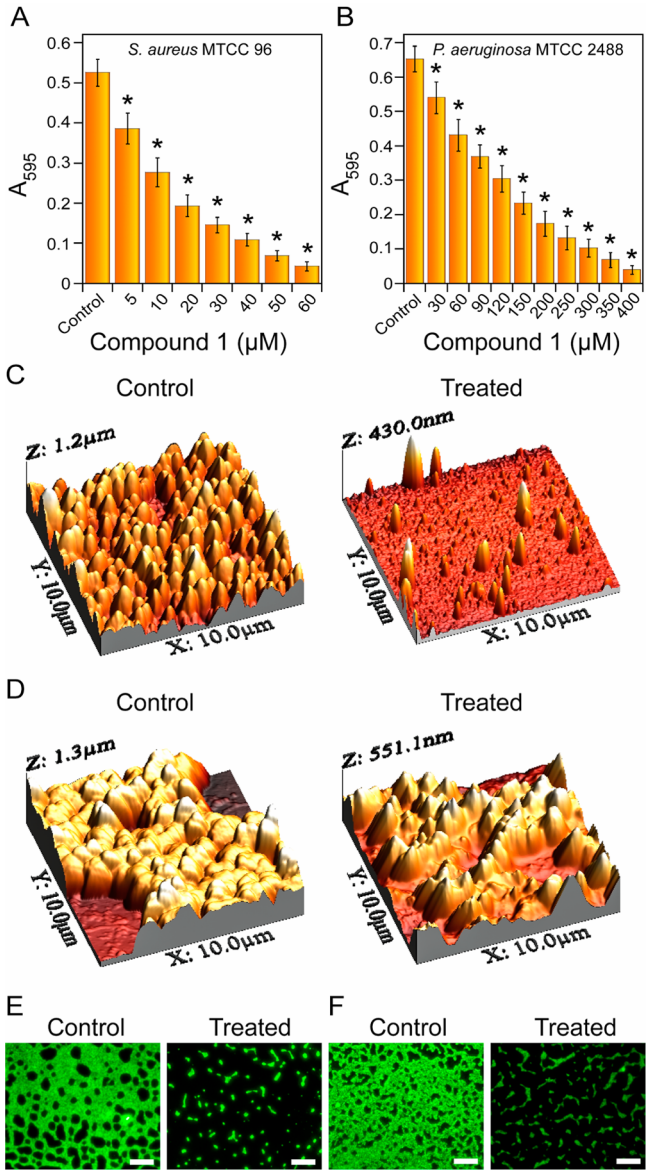

Figure 2. Crystal violet assay to assess the antibiofilm activity of **compound 1** against (A) *S. aureus* MTCC 96 biofilm and (B) *P. aeruginosa* MTCC 2488 biofilm. ∗ indicates the p value <0.001 in ANOVA. Three-dimensional topography AFM images of (C) *S. aureus* MTCC 96 biofilm (control and treated with 30 μM **compound 1**) and (D) *P. aeruginosa* MTCC 2488 biofilm (control and treated with 200 μM **compound 1**). AFM images are shown for an area of 10 μm × 10 μm. Fluorescence microscope analysis of cFDA-SE labeled (E) *S. aureus* MTCC 96 biofilm (control and treated with 30 μM **compound 1**) and (F) *P. aeruginosa* MTCC 2488 biofilm (control and treated with 200 μM **compound 1**). Scale bar for the images is 50 μm.

results were also observed in FESEM analysis, congo red staining, and PI staining in the case of *P. aeruginosa* biofilm treated with **compound 1**. Collectively, the aforementioned results suggested that **compound 1** could pervade through the biofilm matrix, access the encased cells, and display its membrane-directed bactericidal activity even in the complex niche of the matrix, resulting in effective annihilation of a preformed biofilm. It was also evident from the results that low concentrations of the amphiphile could effectively eliminate *S. aureus* biofilm, while eradication of *P. aeruginosa* biofilm required substantially higher concentrations of the amphiphile.

dx.doi.org/10.1021/am504779t | *ACS Appl. Mater. Interfaces* 2014, 6, 16384−16394

Eradication of Biofilm by Antibiotics in Combination with Compound 1. Bacterial biofilms display remarkable resistance against conventional antibiotic-mediated therapy as compared to the planktonic cells and are thus largely implicated in chronic and intractable infections.[1,10,38−40] For instance, biofilm of the opportunistic pathogen *Pseudomonas aeruginosa* is known to be associated with chronic lung infection in cystic fibrosis (CF) patients.[11,12] Tobramycin is an aminoglycoside antibiotic, which is often deployed for mitigation of *P. aeruginosa* biofilm.[41] However, the presence of an extracellular matrix as a diffusion barrier and limited antibiotic penetration is a major bottleneck in tobramycin-mediated antibiofilm therapy.[42,43] In the present study, we observed that **compound 1** at high concentrations (200 μM) prevailed over the matrix barrier and could eradicate established *P. aeruginosa* biofilm (Figure 2). From a therapeutic standpoint, usage of such high concentrations of the amphiphile to eliminate *P. aeruginosa* biofilm is unsuitable as it may entail unwarranted host cell toxicity.[25] However, on the basis of its potent membrane-directed antibacterial activity, it was envisaged that the amphiphile can perhaps be used at low concentrations to sensitize the matrix encased cells of biofilm and render them susceptible to the action of antibiotics in combination therapy. To test this theory, treatment of established biofilms of *P. aeruginosa* and *S. aureus* by a combination of **compound 1** and tobramycin or gentamicin, respectively, was pursued. These antibiotics were chosen based on their known activity against the respective target bacteria.[41,44] Initially the MIC of **compound 1**, gentamicin, and tobramycin against the planktonic cells of respective target bacteria were determined (Supporting Information, Table S1). Treatment of *P. aeruginosa* biofilm with 10−30 μM **compound 1** resulted in 5.7%−21.5% eradication of biofilm biomass, respectively (Figure 3A,B). When *P. aeruginosa* biofilm was treated with 0.08 μg/mL and 0.625 μg/mL tobramycin, the corresponding eradication of biofilm biomass amounted to 25.3% and 56.8%, respectively (Figure 3A,B). Interestingly, in the combinatorial assays, the elimination of biofilm biomass was distinctly higher as compared to treatment with either the amphiphile or antibiotic. For instance, treatment of *P. aeruginosa* biofilm with 0.625 μg/mL tobramycin in combination with **compound 1** (10 μM, 20 μM, and 30 μM) resulted in 73%, 83%, and 89% eradication in biofilm biomass, respectively (Figure 3B). Evidence for superior eradication of *P. aeruginosa* biofilm in combination treatment was captured in FESEM analysis, which suggested extensive disruption of cells and breach of cell−cell adhesion as well as in congo red staining, which indicated a dramatic reduction in *P. aeruginosa* biofilm EPS (Figure 3C). Eradication of *S. aureus* biofilm in the presence of **compound 1** and gentamicin further substantiated the ability of the amphiphile to abolish biofilm in combination with an antibiotic (Supporting Information, Figure S4). Combination therapy with bactericidal agents and antibiotics for alleviation of biofilm has been reported in previous studies.[45−47]

It is also significant to mention here that in the present study, the combination of **compound 1** and tobramycin at the selected concentrations did not impair the viability of a model human cell line (HeLa cells) in an *in vitro* cytotoxicity assay (Supporting Information, Figure S5). This finding reflects the merit of the amphiphile as an adjuvant in combination therapy for eradication of *P. aeruginosa* biofilm. Furthermore, it offered an opportunity to reduce the levels of tobramycin for effective elimination of biofilm. This is significant given that use of tobramycin at high concentrations may lead to gratuitous toxic effects.[48]

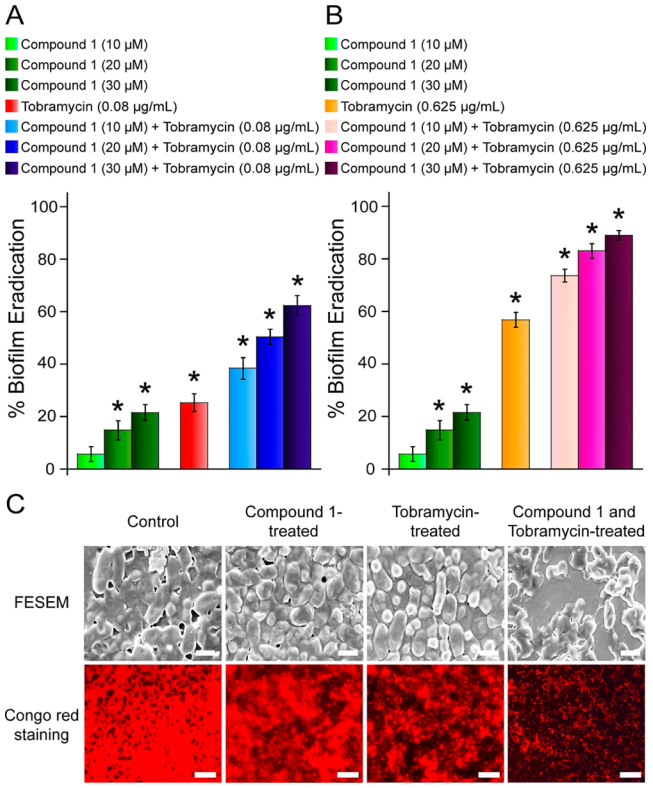

Figure 3. Effect of combined treatment of **compound 1** with (A) 0.08 μg/mL tobramycin and (B) 0.625 μg/mL tobramycin on *P. aeruginosa* MTCC 2488 biofilm measured by crystal violet assay. Statistically significant values derived by ANOVA are indicated by asterisk marks. * indicates p value <0.001. (C) Representative FESEM images and congo red stained fluorescence microscope images of *P. aeruginosa* MTCC 2488 biofilm treated with 30 μM **compound 1**, 0.08 μg/mL tobramycin, and 30 μM **compound 1** in combination with 0.08 μg/mL tobramycin. Scale bar for FESEM and fluorescence microscope images are 1.0 and 50 μm, respectively.

Compound 1-Loaded HSA Nanocarrier (C1-HNC). The antibiofilm potential of **compound 1** was quite promising. However, to explore the prospect of **compound 1** in antibiofilm therapy, generation of a delivery vehicle that ensures sustained release of the payload would be paramount. In this regard, it was conceived that development of a **compound 1**-loaded nanocarrier, which can infiltrate the biofilm matrix is likely to render a sustained and localized release of the amphiphile, leading to effective eradication of biofilm. However, it was critical to ensure that the nanocarrier itself was nontoxic and suitable for potential therapeutic applications. In line with this rationale, a human serum albumin (HSA)-based nanocarrier for **compound 1** was developed, given the biocompatible attribute and extensive use of this serum protein as a nanocarrier in biomedical applications.[35,36] Following a desolvation process,[49] HSA nanoparticles (HNPs) were obtained in high yield of nearly 80% as measured by Bradford assay. FESEM and TEM analysis revealed characteristic spherical-shaped HNPs (Figure 4A,B), with an average particle size of 220 nm (Figure 4C). **Compound 1**-loaded HSA nanocarrier (C1-HNC) was prepared by incubating preformed HNPs with varying concentrations of **compound 1** in order to facilitate uptake

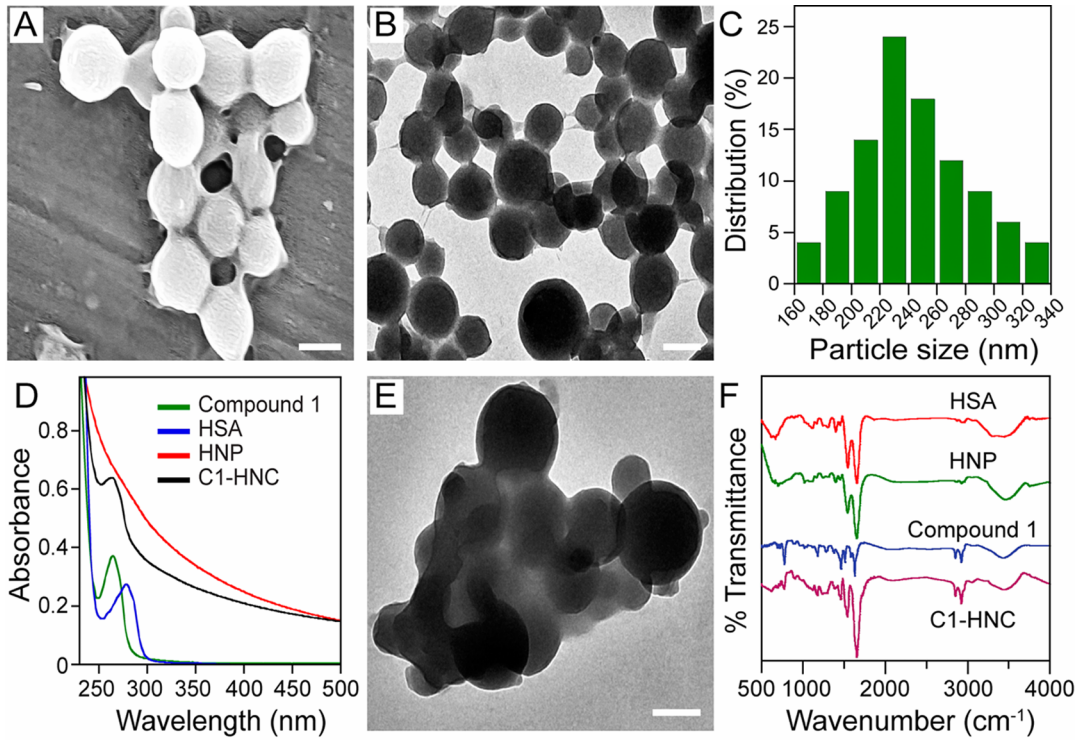

Figure 4. (A) FESEM image of HSA nanoparticles (HNPs). (B) TEM image of HNPs. (C) Determination of particle size of HNPs using ImageJ software (http://rsb.info.nih.gov/ij). Characterization of **compound 1**-loaded HSA nanocarrier (C1-HNC) by (D) UV–visible absorbance spectroscopy, (E) TEM analysis, and (F) FTIR analysis. The scale bar for the images in panel A, B, and E is 200 nm.

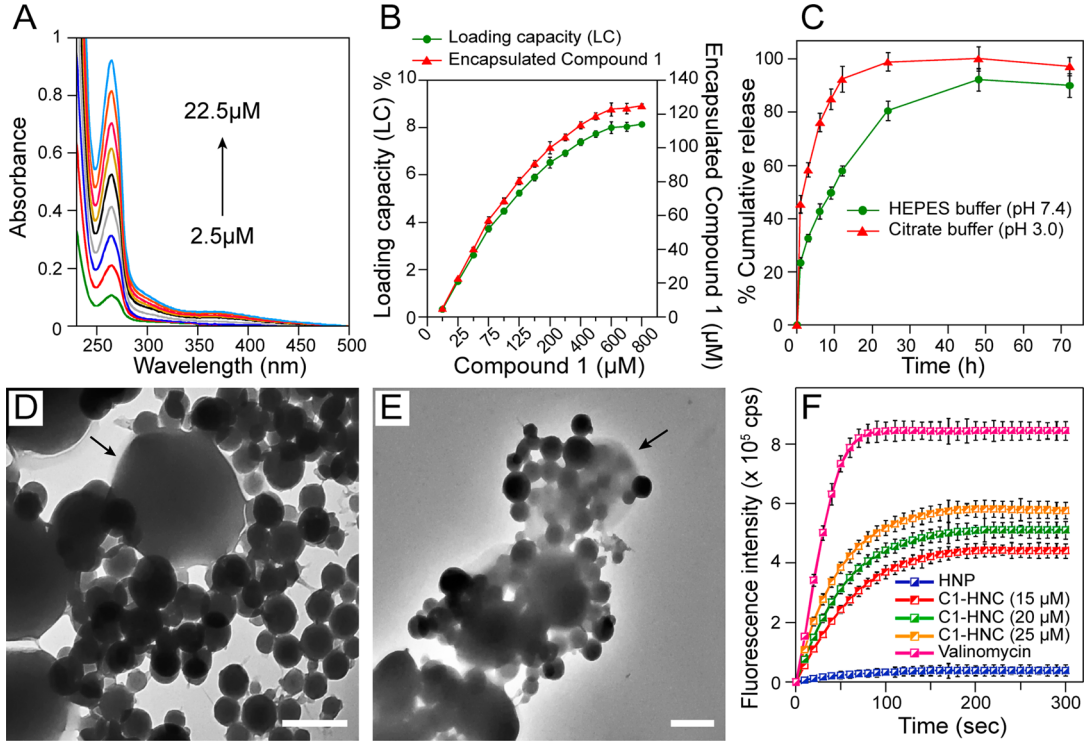

Figure 5. (A) UV–visible absorption spectra of varying concentrations of **compound 1**. (B) Loading capacity (LC) and amount of encapsulation of **compound 1** in HSA nanoparticles. (C) *In vitro* release kinetics of **compound 1** from C1-HNC incubated in 10 mM HEPES buffer (pH 7.4) and 100 mM citrate buffer (pH 3.0). TEM images of *S. aureus* MTCC 96 cells treated with (D) HNPs and (E) C1-HNC. Arrow in panel D indicates a typical spherical shaped *S. aureus* cell and cluster of smaller size HNPs in the vicinity. Arrow in panel E indicates disintegration and loss of electron density in *S. aureus* cell treated with C1-HNC. Scale bar for the TEM images is 0.2 μm. (F) $DiSC_3$5-based membrane depolarization assay for *S. aureus* MTCC 96 cells treated with varying concentrations of C1-HNC. Cells treated with 30 μM valinomycin were used as positive control in the assay.

dx.doi.org/10.1021/am504779t | *ACS Appl. Mater. Interfaces* 2014, 6, 16384–16394

of the amphiphile. UV−visible spectra of C1-HNC revealed an absorbance peak at 265 nm, which suggested the presence of **compound 1** in HSA nanocarrier (Figure 4D). TEM analysis of C1-HNC indicated aggregates of nanoparticles (Figure 4E) perhaps due to the strong hydrophobic interactions. Loading of HNPs with **compound 1** was further corroborated by FTIR spectroscopic analysis of C1-HNC, wherein characteristic stretching frequencies of the HSA protein as well as **compound 1** was conserved (Figure 4F).

Prior to estimating the amphiphile loading capacity (LC) of HNPs, a concentration-dependent UV−visible absorption spectra of **compound 1** was measured (Figure 5A), which yielded a linear calibration plot (Supporting Information, Figure S6). The loading capacity (LC) of HNPs exhibited a progressive increase with increment in the concentration of **compound 1** and a saturation effect was observed at around 600 μM of the amphiphile (Figure 5B). At the highest concentration of **compound 1** (800 μM), the LC of HNPs and the amount of encapsulated **compound 1** was estimated to be around 8.2% and 125 μM, respectively (Figure 5B). In order to assess the therapeutic potential of **compound 1**-loaded HSA nanocarrier, studies on the *in vitro* release of **compound 1** from the payload nanocarrier was pertinent. The *in vivo* efficacy of a bactericidal molecule is generally influenced by its serum concentration and binding to plasma protein and tissue and thus it is a common practice to employ antibacterials at concentrations exceeding their MIC for effective *in vivo* elimination of target bacteria.[50−53] On the basis of this premise, the *in vitro* release kinetics of **compound 1** was studied with C1-HNC loaded with a high concentration of **compound 1** (125 μM). At a physiological pH of 7.4, a slow release of the amphiphile from C1-HNC was observed, with around 60% release following 12 h of incubation (Figure 5C). Subsequently, a progressive increase in the release of **compound 1** was observed with the estimated cumulative release reaching a plateau of around 92% after 48 h. In acidic pH (pH 3.0), release of **compound 1** from C1-HNC was rapid, as compared to the profile observed at pH 7.4 (Figure 5C).

Following successful encapsulation and *in vitro* release of **compound 1** from the HSA-based nanocarrier, it was pertinent to ascertain whether the loaded amphiphile retained its characteristic bactericidal activity upon encapsulation. To pursue this goal, *S. aureus* MTCC 96 was selected as a model Gram-positive target bacteria. As a Gram-negative bacterium, *E. coli* MTCC 433 was used as a target in lieu of *P. aeruginosa* MTCC 2488. This was based on the lower MIC of **compound 1** against *E. coli* MTCC 433 (64 μM or 41.68 μg/mL)[25] as compared to the MIC against *P. aeruginosa* MTCC 2488 (Supporting Information, Table S1). Moreover, given the higher concentration of **compound 1** required for annihilation of *P. aeruginosa*, therapeutic usage of C1-HNC against this target bacterium entails circumspection as high concentration of the amphiphile may bear cytotoxic implications.[25]A dose-dependent impairment of bacterial cell viability was observed upon treatment with C1-HNC as evident from the time-kill curves (Supporting Information, S7A,B). TEM analysis suggested that HNPs alone were devoid of any antibacterial activity as evident from the retention of the characteristic morphology in *S. aureus* cells bound by a cluster of smaller size HNPs (Figure 5D). However, treatment with C1-HNC resulted in disintegration and leakage of cellular contents, which was apparent in the significant morphological distortion and loss of electron density in the target bacterial cells (Figure 5E). Interestingly, C1-HNC could also render a rapid and dose-dependent membrane depolarization in *S. aureus* and *E. coli* cells (Figure 5F and Supporting Information, Figure S7C), which is a signature activity of **compound 1**.[25] The antibacterial activity of C1-HNC likely is a consequence of release of the payload (**compound 1**). To verify this possibility, the bactericidal activity of released **compound 1** was also evaluated. In essence, C1-HNC (loaded with 125 μM **compound 1**) was subjected to the experimental conditions analogous to *in vitro* release kinetics in 10 mM HEPES buffer (pH 7.4) for 48 h. Subsequently, the recovered supernatant was diluted to achieve a **compound 1** concentration of 15 μM, 30 μM, and 45 μM in separate sets and their antibacterial activity was tested against representative Gram-positive and Gram-negative bacteria. A concentration-dependent killing was explicit for all the target bacterial strains (Supporting Information, Figure S8). It may be mentioned that among the target bacterial strains, **compound 1** was most potent against *S. aureus* MTCC 96, which is a presumptive methicillin-resistant *Staphylococcus aureus* (MRSA) strain.[24]

Antibiofilm Activity of compound 1-Loaded HSA Nanocarrier (C1-HNC). The significant antibacterial activity exhibited by C1-HNC against *S. aureus* MTCC 96 suggested that the amphiphile-loaded nanocarrier could perhaps be deployed for eradication of biofilm formed by this bacterium. Interestingly, an MTT-based colorimetric assay indicated a systematic and significant loss in the viability of *S. aureus* biofilm-associated cells upon treatment with increasing concentrations of C1-HNC (Figure 6A). FESEM analysis of untreated as well as HNP-treated *S. aureus* biofilm revealed a cluster of cells displaying the characteristic spherical morphology and prominent cell−cell adhesion typically associated with biofilm formation (Figure 6B). In the case of HNP-treated *S.*

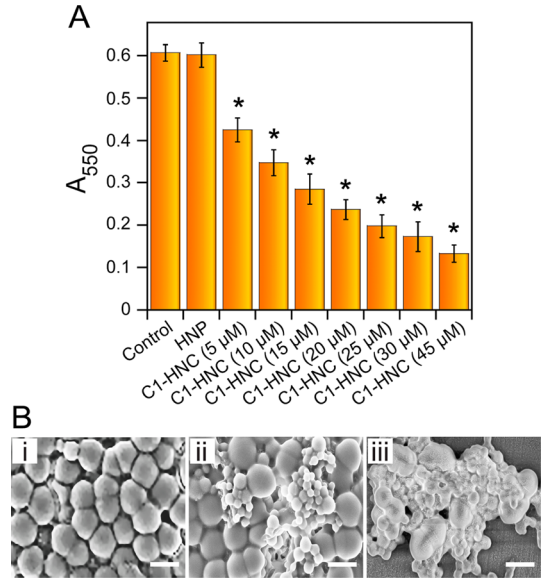

Figure 6. (A) MTT assay to ascertain the effect of C1-HNC on the viability of *S. aureus* MTCC 96 biofilm. The concentrations of **compound 1** in C1-HNC samples are indicated in parentheses. Statistically significant values derived by ANOVA are indicated by asterisk marks. ∗ indicates p value <0.001. (B) FESEM images of (i) untreated *S. aureus* MTCC 96 biofilm and *S. aureus* MTCC 96 biofilm treated with (ii) HNPs and (iii) C1-HNC (corresponding to 30 μM **compound 1** concentration). Scale bar for the images is 1.0 μm.

aureus biofilm, a bunch of smaller size HNPs adhering on to *S. aureus* biofilm could be readily deciphered (Figure 6B, panel ii). Interestingly, the antibiofilm activity of C1-HNC could be captured in FESEM analysis, wherein a distinct disruption of *S. aureus* biofilm manifested in the form of gross morphological perturbation of cells and breach of the typical cell−cell adhesion (Figure 6B, panel iii). These findings suggested that **compound 1**-loaded HSA nanocarrier could invade the *S. aureus* biofilm matrix to establish contact with the embedded cells, and the antibiofilm activity of the nanocarrier is perhaps accounted for by the release of the payload (**compound 1**) and its ensuing action on biofilm-associated cells.

Eradication of Catheter-Associated Biofilm. Medical devices such as intravascular and urinary catheters are regarded as citadels of the modern healthcare armory. However, they are highly vulnerable to colonization by bacterial biofilm that display remarkable resistance to antibiotic-mediated therapy leading to the development of persistent catheter-associated infections.[1,5,17,54] Although a gamut of strategies based on surface coating with antibacterials has been proposed to prevent biofilm formation on catheters,[55−57] eradication of catheter-associated biofilm infection remains a serious therapeutic challenge and underscores the pressing need of antibacterials that can act on established biofilms on a catheter surface. The potent activity of **compound 1** on preformed biofilms motivated us to deploy the amphiphile for abolition of catheter-associated biofilm. To this end, *S. aureus* was chosen as the model biofilm forming organism and grown on Foley's urinary catheter, given its propensity to adhere to the catheter surface and its relevance in catheter-associated urinary tract infections.[58] Interestingly, a formazan-based MTT assay revealed a significant dose-dependent elimination of established *S. aureus* biofilm from the surface of the catheter upon treatment with **compound 1** as well as C1-HNC albeit to a marginally lesser extent (Figure 7A). Eradication of *S. aureus* biofilm from the catheter surface is likely to be a function of the local concentration of the amphiphile available at the abiotic surface. In the case of treatment with **compound 1**, the amphiphile is readily available for its action on the biofilm, whereas in the case of C1-HNC, release of the amphiphile from the nanocarrier is a prerequisite for its action on the established biofilm. This may account for the slightly higher eradication of biofilm from the surface of the catheter treated with **compound 1** as compared to treatment with C1-HNC. Evidence for antibiofilm activity of the amphiphile as well as C1-HNC on the catheter surface was also obtained from FESEM analysis. Densely packed adherent cells of *S. aureus* typically associated with biofilm architecture were conspicuous on the surface of an untreated Foley's urinary catheter (Figure 7B, panel ii). Treatment of the biofilm-colonized catheter with **compound 1** resulted in dramatic eradication of *S. aureus* biofilm from the surface of the catheter (Figure 7B, panel iii). Eradication of *S. aureus* biofilm from the catheter surface was also distinct in the case of C1-HNC treatment, and the breakdown of the biofilm network and loss of typical cell morphology was evident (indicated by an arrow in Figure 7B, panel iv). Collectively, the findings of these experiments highlighted the ability of the amphiphile and amphiphile-loaded HSA nanocarrier to annihilate established *S. aureus* biofilm from a clinically pertinent surface.

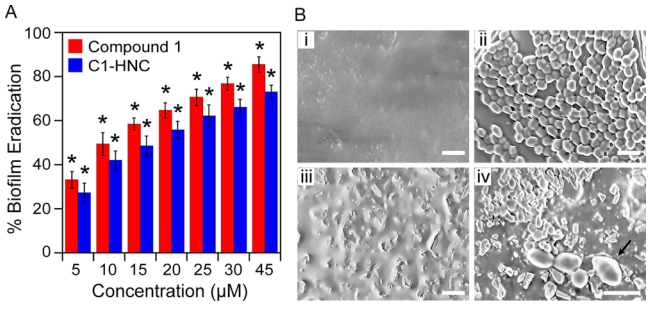

Figure 7. (A) MTT assay to ascertain eradication of pregrown *S. aureus* MTCC 96 biofilm from the surface of a Foley's urinary catheter treated with **compound 1** and C1-HNC. (B) FESEM images of Foley's urinary catheter segments indicating (i) bare catheter surface, (ii) untreated *S. aureus* biofilm, (iii) *S. aureus* biofilm treated with 30 μM **compound 1**, and (iv) *S. aureus* biofilm treated with C1-HNC (corresponding to 30 μM **compound 1**). The arrow in panel iv indicates a damaged cell. The scale bar for the FESEM images is 2.0 μm.

In the context of potential therapeutic application of **compound 1**-loaded HSA nanocarrier for eradication of established *S. aureus* biofilm from a catheter surface, it is critical that the developed payload nanocarrier should not render any detrimental cytotoxic effect on host cells. To this end, HeLa cells were chosen as model human cells to ascertain the cytotoxic effect of C1-HNC. Interestingly, an MTT-based assay revealed that the amphiphile-loaded nanocarrier did not influence the metabolic activity and viability of HeLa cells (Figure 8A) even at concentrations (30 μM and 45 μM **compound 1**), which rendered effective eradication of *S. aureus* biofilm from the catheter surface (Figure 7A). Fluorescence microscope analysis of HeLa cells treated with C1-HNC (30 μM) indicated the presence of a large number of cFDA-SE stained cells, indicating that the cells were viable (Figure 8B). Furthermore, HeLa cells treated with either HNPs or C1-HNC did not exhibit any PI staining, which suggested the lack of any membrane damage. Collectively, MTT assay and fluorescence microscope analysis indicated the nontoxic nature of compound 1-loaded HSA nanocarrier and highlighted the potential of the developed nanocarrier in device-associated antibiofilm therapy.

CONCLUSIONS

The menace of bacterial biofilms in the healthcare regime is ominous. The high incidence of life-threatening biofilm-associated chronic infections has triggered a critical demand for antibiofilm therapeutics as conventional interventions using antibiotics are turning out to be increasingly futile. Although a large number of synthetic molecules that inhibit the formation of bacterial biofilms have been developed, we have demonstrated in the present study that a potent antibacterial synthetic amphiphile (**compound 1**) can be employed either alone, in combination with antibiotics, or through an albumin-based nanocarrier system to efficiently annihilate established bacterial biofilms. From a therapeutic perspective, development of such a biocompatible nanocarrier empowered with a potent antibiofilm payload augers well in addressing the significantly greater clinical challenge of treating chronic infections caused by established and defiant biofilms.

Medical devices such as catheters are extensively used and largely recognized as a bastion of the modern healthcare arsenal. However, biofilm growth on catheters leads to infections, which are often recalcitrant to antibiotic therapy and require arduous surgical interventions. In this regard, the ability of **compound 1**-loaded nontoxic nanocarrier to display

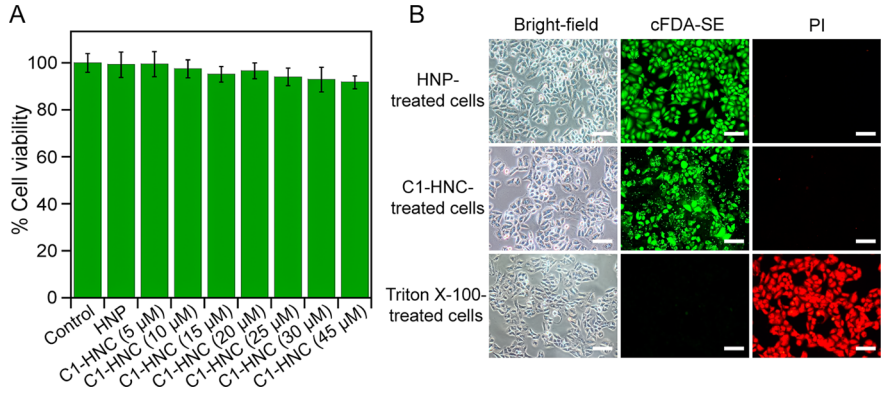

Figure 8. (A) MTT-based assay to determine the cytotoxic effect of C1-HNC on HeLa cells. The concentrations of **compound 1** in C1-HNC are mentioned in parentheses. (B) Fluorescence microscope images of HNP-treated, C1-HNC-treated, and Triton X-100-treated HeLa cells. The scale bar for the images is 50 μm.

antibiofilm activity on a clinically relevant surface and eradicate established biofilm from a model catheter highlights the potential of the developed nanocarrier in device-associated antibiofilm therapy. In the future, it would be interesting to employ the amphiphile-loaded nanocarrier in conjunction with appropriate materials chemistry to develop a surface active coating for catheters that enables controlled-release of the amphiphile and prevents colonization of such implants by biofilms.

■ ASSOCIATED CONTENT

Supporting Information

Additional experimental procedures, antibiofilm activity of **compound** 1, AFM images, FESEM and fluorescence microscope images, combination effect of **compound 1** and gentamicin, cytotoxicity for combination of **compound 1** and tobramycin, calibration plot for **compound 1**, time-kill curves, $DiSC_3$5-based assay, antibacterial activity of **compound 1** released from C1-HNC, and MIC of **compound 1**, gentamicin, and tobramycin. This material is available free of charge via the Internet at http://pubs.acs.org.

■ AUTHOR INFORMATION

Corresponding Authors

*E-mail: gdas@iitg.ernet.in. Fax: + 91-361-2582349. Phone: +91-361-2582313.
*E-mail: aramesh@iitg.ernet.in. Fax: +91-361-2582249. Phone: +91-361- 2582205.

Notes

The authors declare no competing financial interest.

■ ACKNOWLEDGMENTS

The authors thank the Science & Engineering Research Board (SR/S1/OC-62/2011), New Delhi, India and Department of Biotechnology (BT/01/NE/PS/08), Government of India for research grants. We thank Chirantan Kar for his assistance in compound synthesis. We also thank Central Instruments Facility, IIT Guwahati for their valuable help in FESEM and AFM analysis. S.G. thanks University Grants Commission (UGC), New Delhi for a research fellowship. D.T. thanks IIT Guwahati, for a research fellowship.

■ REFERENCES

(1) Costerton, J. W.; Stewart, P. S.; Greenberg, E. P. Bacterial Biofilms: A Common Cause of Persistent Infections. *Science* **1999**, *284*, 1318−1322.
(2) Archer, N. K.; Mazaitis, M. J.; Costerton, W.; Leid, J. G.; Powers, M. E.; Shirtliff, M. E. *Staphylococcus aureus* Biofilms: Properties, Regulation and Roles in Human Disease. *Virulence* **2011**, *2*, 445−459.
(3) Flemming, H. C.; Wingender, J. The Biofilm Matrix. *Nat. Rev. Microbiol.* **2010**, *8*, 623−633.
(4) Kostakioti, M.; Hadjifrangiskou, M.; Hultgren, S. J. Bacterial Biofilms: Development, Dispersal, and Therapeutic Strategies in the Dawn of the Postantibiotic Era. *Cold Spring Harb. Perspect. Med.* **2013**, *3*, a010306.
(5) Donlan, R. M.; Costerton, J. W. Biofilms: Survival Mechanisms of Clinically Relevant Microorganisms. *Clin. Microbiol. Rev.* **2002**, *15*, 167−193.
(6) Bordi, C.; Bentzmann, S. D. Hacking into Bacterial Biofilms: A New Therapeutic Challenge. *Ann. Intensive Care* **2011**, *1*, 19.
(7) Otto, M. Staphylococcal Biofilms. *Curr. Top. Microbiol. Immunol.* **2008**, *322*, 207−228.
(8) Mann, E. E.; Wozniak, D. J. *Pseudomonas* Biofilm Matrix Composition and Niche Biology. *FEMS Microbiol. Rev.* **2012**, *36*, 893−916.
(9) Parsek, M. R.; Singh, P. K. Bacterial Biofilms: An Emerging Link to Disease Pathogenesis. *Annu. Rev. Microbiol.* **2003**, *57*, 677−701.
(10) Davies, D. Understanding Biofilm Resistance to Antibacterial Agents. *Nat. Rev. Drug Discovery* **2003**, *2*, 114−122.
(11) Wagner, V. E.; Iglewski, B. H. *P. aeruginosa* Biofilms in CF Infection. *Clin. Rev. Allergy Immunol.* **2008**, *35*, 124−134.
(12) Gomez, M. I.; Prince, A. Opportunistic Infections in Lung Disease: *Pseudomonas* Infections in Cystic Fibrosis. *Curr. Opin. Pharmacol.* **2007**, *7*, 244−251.
(13) Arciola, C. R.; Campoccia, D.; Speziale, P.; Montanaro, L.; Costerton, J. W. Biofilm Formation in *Staphylococcus* Implant Infections. A Review of Molecular Mechanisms and Implications for Biofilm-Resistant Materials. *Biomaterials* **2012**, *33*, 5967−5982.
(14) Trautner, B. W.; Darouiche, R. O. Catheter-Associated Infections: Pathogenesis Affects Prevention. *Arch. Int. Med.* **2004**, *164*, 842−850.
(15) Warren, J. W. Catheter-Associated Urinary Tract Infections. *Int. J. Antimicrob. Agents* **2001**, *17*, 299−303.
(16) Hoiby, N.; Bjarnsholt, T.; Givskov, M.; Molin, S.; Ciofu, O. Antibiotic Resistance of Bacterial Biofilms. *Int. J. Antimicrob. Agents* **2010**, *35*, 322−332.
(17) Stewart, P. S.; Costerton, J. W. Antibiotic Resistance of Bacteria in Biofilms. *Lancet* **2001**, *358*, 135−138.
(18) Fux, C. A.; Costerton, J. W.; Stewart, P. S.; Stoodley, P. Survival Strategies of Infectious Biofilms. *Trends Microbiol.* **2005**, *13*, 34−40.

(19) Broderick, A. H.; Breitbach, A. S.; Frei, R.; Blackwell, H. E.; Lynn, D. M. Surface-Mediated Release of a Small-Molecule Modulator of Bacterial Biofilm Formation: A Non-Bactericidal Approach to Inhibiting Biofilm Formation in *Pseudomonas aeruginosa*. *Adv. Healthcare Mater.* **2013**, *2*, 993−1000.
(20) Bunders, C.; Cavanagh, J.; Melander, C. Flustramine Inspired Synthesis and Biological Evaluation of Pyrroloindoline Triazole Amides as Novel Inhibitors of Bacterial Biofilms. *Org. Biomol. Chem.* **2011**, *9*, 5476−5481.
(21) Geske, G. D.; Wezeman, R. J.; Siegel, A. P.; Blackwell, H. E. Small Molecule Inhibitors of Bacterial Quorum Sensing and Biofilm Formation. *J. Am. Chem. Soc.* **2005**, *127*, 12762−12763.
(22) Worthington, R. J.; Richards, J. J.; Melander, C. Small Molecule Control of Bacterial Biofilms. *Org. Biomol. Chem.* **2012**, *10*, 7457−7474.
(23) Singh, V.; Arora, V.; Alam, J. M.; Garey, K. W. Inhibition of Biofilm Formation by Esomeprazole in *Pseudomonas aeruginosa* and *Staphylococcus aureus*. *Antimicrob. Agents Chemother.* **2012**, *56*, 4360−4364.
(24) Vudumula, U.; Adhikari, M. D.; Ojha, B.; Goswami, S.; Das, G.; Ramesh, A. Tuning the Bactericidal Repertoire and Potency of Quinoline-based Amphiphiles for Enhanced Killing of Pathogenic Bacteria. *RSC Adv.* **2012**, *2*, 3864−3871.
(25) Goswami, S.; Adhikari, M. D.; Kar, C.; Thiyagarajan, D.; Das, G.; Ramesh, A. Synthetic Amphiphiles as Therapeutic Antibacterials: Lessons on Bactericidal Efficacy and Cytotoxicity and Potential Application as an Adjuvant in Antimicrobial Chemotherapy. *J. Mater. Chem. B* **2013**, *1*, 2612−2623.
(26) Thiyagarajan, D.; Goswami, S.; Kar, C.; Das, G.; Ramesh, A. A Prospective Antibacterial for Drug-Resistant Pathogens: A Dual Warhead Amphiphile Designed to Track Interactions and Kill Pathogenic Bacteria by Membrane Damage and Cellular DNA Cleavage. *Chem. Commun.* **2014**, *50*, 7434−7436.
(27) Zhang, L.; Pornpattananangkul, D.; Hu, C. M.; Huang, C. M. Development of Nanoparticles for Antimicrobial Drug Delivery. *Curr. Med. Chem.* **2010**, *17*, 585−594.
(28) Risbud, M. V.; Hardikar, A. A.; Bhat, S. V.; Bhonde, R. R. pH-Sensitive Freeze-Dried Chitosan−Polyvinyl Pyrrolidone Hydrogels as Controlled Release System for Antibiotic Delivery. *J. Controlled Release* **2000**, *68*, 23−30.
(29) Alphandary, H. P.; Andremont, A.; Couvreur, P. Targeted Delivery of Antibiotics Using Liposomes and Nanoparticles: Research and Applications. *Int. J. Antimicrob. Agents* **2000**, *13*, 155−168.
(30) Applerot, G.; Lellouche, J.; Perkas, Nina.; Nitzan, Y.; Gedanken, A.; Banin, E. ZnO Nanoparticle-Coated Surfaces Inhibit Bacterial Biofilm Formation and Increase Antibiotic Susceptibility. *RSC Adv.* **2012**, *2*, 2314−2321.
(31) Adhikari, M. D.; Goswami, S.; Panda, B. R.; Chattopadhyay, A.; Ramesh, A. Membrane-Directed High Bactericidal Activity of (Gold Nanoparticle)−Polythiophene Composite for Niche Applications Against Pathogenic Bacteria. *Adv. Healthcare Mater.* **2013**, *2*, 599−606.
(32) Slomberg, D. L.; Lu, Y.; Broadnax, A. D.; Hunter, R. A.; Carpenter, A. W.; Schoenfisch, M. H. Role of Size and Shape on Biofilm Eradication for Nitric Oxide-Releasing Silica Nanoparticles. *ACS Appl. Mater. Interfaces* **2013**, *5*, 9322−9329.
(33) Shimanovich, U.; Bernardes, G. J. L.; Knowles, T. P. J.; Cavaco-Paulo, A. Protein Micro- and Nano-Capsules for Biomedical Applications. *Chem. Soc. Rev.* **2014**, *43*, 1361−1371.
(34) Elzoghby, A. O.; Samy, W. M.; Elgindy, N. A. Protein-Based Nanocarriers as Promising Drug and Gene Delivery Systems. *J. Controlled Release* **2012**, *161*, 38−49.
(35) Kratz, F. Albumin as a Drug Carrier: Design of Prodrugs, Drug Conjugates and Nanoparticles. *J. Controlled Release* **2008**, *132*, 171−183.
(36) Elzoghby, A. O.; Samy, W. M.; Elgindy, N. A. Albumin-based Nanoparticles as Potential Controlled Release Drug Delivery Systems. *J. Controlled Release* **2012**, *157*, 168−182.
(37) Lambert, P. A. Mechanisms of Antibiotic Resistance in *Pseudomonas aeruginosa*. *J. R. Soc. Med.* **2002**, *95* (Suppl. 41), 22−26.
(38) Stewart, P. S. Mechanisms of Antibiotic Resistance in Bacterial Biofilms. *Int. J. Med. Microbiol.* **2002**, *292*, 107−113.
(39) Hogan, D.; Kolter, R. Why are Bacteria Refractory to Antimicrobials? *Curr. Opin. Microbiol.* **2002**, *5*, 472−477.
(40) Church, D.; Elsayed, S.; Reid, O.; Winston, B.; Lindsay, R. Burn Wound Infections. *Clin. Microbiol. Rev.* **2006**, *19*, 403−434.
(41) Anderson, G. G.; Moreau-Marquis, S.; Stanton, B. A.; O'Toole, G. A. *In Vitro* Analysis of Tobramycin-Treated *Pseudomonas aeruginosa* Biofilms on Cystic Fibrosis-Derived Airway Epithelial Cells. *Infect. Immun.* **2008**, *76*, 1423−1433.
(42) Tseng, B. S.; Zhang, W.; Harrison, J. J.; Quach, T. P.; Song, J. L.; Penterman, J.; Singh, P. K.; Chopp, D. L.; Packman, A. I.; Parsek, M. R. The Extracellular Matrix Protects *Pseudomonas aeruginosa* Biofilms by Limiting the Penetration of Tobramycin. *Environ. Microbiol.* **2013**, *15*, 2865−2878.
(43) Walters, M. C., III; Roe, F.; Bugnicourt, A.; Franklin, M. J.; Stewart, P. S. Contributions of Antibiotic Penetration, Oxygen Limitation, and Low Metabolic Activity to Tolerance of *Pseudomonas aeruginosa* Biofilms to Ciprofloxacin and Tobramycin. *Antimicrob. Agents Chemother.* **2003**, *47*, 317−323.
(44) Olson, K. M.; Starks, C. M.; Williams, R. B.; O'Neil-Johnson, M.; Huang, Z.; Ellis, M.; Reilly, J. E.; Eldridge, G. R. Novel Pentadecenyl Tetrazole Enhances Susceptibility of Methicillin-Resistant *Staphylococcus aureus* Biofilms to Gentamicin. *Antimicrob. Agents Chemother.* **2011**, *55*, 3691−3695.
(45) Rogers, A.; Huigens, R. W.; Cavanagh, J.; Melander, C. Synergistic Effects Between Conventional Antibiotics and 2-Amino-imidazole-Derived Antibiofilm Agents. *Antimicrob. Agents Chemother.* **2010**, *54*, 2112−2118.
(46) Kim, J.; Pitts, B.; Stewart, P. S.; Camper, A.; Yoon, J. Comparison of the Antimicrobial Effects of Chlorine, Silver Ion, and Tobramycin on Biofilm. *Antimicrob. Agents Chemother.* **2008**, *52*, 1446−1453.
(47) Drew, K. R. P.; Sanders, L. K.; Culumber, Z. W.; Zribi, O.; Wong, G. C. L. Cationic Amphiphiles Increase Activity of Amino-glycoside Antibiotic Tobramycin in the Presence of Airway Polyelectrolytes. *J. Am. Chem. Soc.* **2009**, *131*, 486−493.
(48) Lode, H. Tobramycin: A Review of Therapeutic Uses and Dosing Schedules. *Curr. Ther. Res.* **1998**, *59*, 420−453.
(49) Langer, K.; Balthasar, S.; Vogel, V.; Dinauer, N.; von Briesen, H.; Schubert, D. Optimization of the Preparation Process for Human Serum Albumin (HSA) Nanoparticles. *Int. J. Pharm.* **2003**, *257*, 169−180.
(50) Craig, W. A. Pharmacokinetic/Pharmacodynamic Parameters: Rationale for Antibacterial Dosing of Mice and Men. *Clin. Infect. Dis.* **1998**, *26*, 1−12.
(51) Mueller, M.; de la Pena, A.; Derendorf, H. Issues in Pharmacokinetics and Pharmacodynamics of Anti-Infective Agents: Kill Curves versus MIC. *Antimicrob. Agents Chemother.* **2004**, *48*, 369−377.
(52) Wispelwey, B. Clinical Implications of Pharmacokinetics and Pharmacodynamics of Fluoroquinolones. *Clin. Infect. Dis.* **2005**, *41*, S127−S135.
(53) Craig, W. A. Basic pharmacodynamics of Antibacterials with Clinical Applications to the Use of β-Lactams, Glycopeptides, and Linezolid. *Infect. Dis. Clin. North Am.* **2003**, *17*, 479−501.
(54) Noimark, S.; Dunnill, C. W.; Wilson, M.; Parkin, I. P. The Role of Surfaces in Catheter-Associated Infections. *Chem. Soc. Rev.* **2009**, *38*, 3435−3448.
(55) Hetrick, E. M.; Schoenfisch, M. H. Reducing Implant-Related Infections: Active Release Strategies. *Chem. Soc. Rev.* **2006**, *35*, 780−789.
(56) Gutiérrez-González, R.; Boto, G. R. Do Antibiotic-Impregnated Catheters Prevent Infection in CSF Diversion Procedures? Review of the literature. *J. Infect.* **2010**, *61*, 9−20.
(57) Furno, F.; Morley, K. S.; Wong, B.; Sharp, B. L.; Arnold, P. L.; Howdle, S. M.; Bayston, R.; Brown, P. D.; Winship, P. D.; Reid, H. J. Silver Nanoparticles and Polymeric Medical Devices: A New Approach

to Prevention of Infection? *J. Antimicrob. Chemother.* **2004**, *54*, 1019−1024.
(58) Muder, R. R.; Brennen, C.; Rihs, J. D.; Wagener, M. M.; Obman, A.; Stout, J. E.; Yu, V. L. Isolation of *Staphylococcus aureus* from the Urinary Tract: Association of Isolation with Symptomatic Urinary Tract Infection and Subsequent Staphylococcal Bacteremia. *Clin. Infect. Dis.* **2006**, *42*, 46−50.